

Symmetry Breaking and Turbulence in Perturbed Plane Couette Flow

Laurette S. Tuckerman

Laboratoire d'Informatique pour la Mécanique et les Sciences de l'Ingénieur (LIMSI-CNRS),
B.P. 133, 91403 Orsay, France
laurette@limsi.fr

Dwight Barkley

Mathematics Institute, University of Warwick, Coventry CV4 7AL, United Kingdom
barkley@maths.warwick.ac.uk

Communicated by H.J.S. Fernando

Received 15 December 2001 and accepted 29 March 2002
Published online 2 October 2002 – © Springer-Verlag 2002

Abstract. Perturbed plane Couette flow containing a thin spanwise-oriented ribbon undergoes a sub-critical bifurcation at $Re \approx 230$ to a steady three-dimensional state containing streamwise vortices. This bifurcation is followed by several others giving rise to a fascinating series of stable and unstable steady states of different symmetries and wavelengths. First, the backwards-bifurcating branch reverses direction and becomes stable near $Re \approx 200$. Then the spanwise reflection symmetry is broken, leading to two asymmetric branches which are themselves destabilized at $Re \approx 420$. Above this Reynolds number, time evolution leads first to a metastable state whose spanwise wavelength is halved and then to complicated time-dependent behavior. These features are in agreement with experiments.

1. Introduction

Research on plane Couette flow has long been hampered by the absence of states intermediate in complexity between laminar plane Couette flow and three-dimensional (3D) turbulence. Intermediate states can be created, however, if a thin wire oriented in the spanwise direction is inserted in an experimental setup (Bottin *et al.* 1997, 1998). No longer subject to Squire's theorem, this perturbed configuration undergoes a bifurcation to a 3D steady or quasi-steady state. The 3D states contain vortices oriented in the streamwise direction and of finite streamwise extent, localized around the ribbon. As the wire radius is reduced, the Reynolds number threshold for the bifurcation and the streamwise extent occupied by the vortices increase, while the range of Reynolds numbers over which the 3D steady states exist decreases.

We have carried out a numerical study corresponding to the experiments of Bottin *et al.* (1997, 1998), focusing primarily on the largest wire radius used. In a previous study (Barkley and Tuckerman, 1999), we carried out a linear and weakly nonlinear stability analysis of this configuration. Here, we present a detailed bifurcation diagram for this case. Our calculations show a rich bifurcation structure with many types

of solutions: stable and unstable; steady, periodic, and aperiodic; and of different symmetries. Some of these solutions persist as the wire radius is reduced.

2. Methods

The time-dependent Navier–Stokes equations have been solved using the spectral element code `Prism` (Henderson and Karniadakis, 1995) written by Henderson. Instead of a wire, we have used a ribbon of infinitesimal streamwise (x) extent whose cross-channel (y) height is taken equal to the diameter of the wire and whose length in the homogeneous transverse (z) direction is infinite. For most of the current study the computational domain is $|x| \leq 32$, $|y| \leq 1$, and $|z| \leq \lambda/2$ where $\lambda = 2\pi/1.3$ is approximately the numerically determined critical wavelength. Periodic boundary conditions have been imposed at $x = \pm 32$ and at $z = \pm \lambda/2$ and no-slip conditions at the channel walls $y = \pm 1$ and at the ribbon $x = 0$, $|y| \leq \rho$. The ratio ρ of the ribbon height to that of the channel is set to $\rho = 0.086$ except where otherwise specified. In the (x, y) directions, we use 24×5 computational elements, each of which is covered by a grid of 7×7 collocation points or interpolating polynomials. In the z direction, we use 32 Fourier modes or gridpoints. (Simulations were also conducted in a reduced spanwise domain $|z| < \lambda/4$ with 16 Fourier modes.) This leads to a total of 143 840 gridpoints or basis functions per velocity component. To compute each asymptotic state required between 500 and 10 000 nondimensional time units (i.e., units of channel width/velocity difference), which in turn required between 3 and 60 CPU hours on each of 16 processors of a Cray T3E. Some tests of the adequacy of our numerical resolution and streamwise domain size are reported in Barkley and Tuckerman (1999). The resolution for complex 3D flows has been checked by increasing the polynomial order from 7 to 11 and the number of Fourier modes from 32 to 64.

3. Bifurcation Scenario for $\rho = 0.086$

Figure 1 shows E_{3D} , the energy in the z -dependent modes for all the steady states we have calculated for $Re < 500$, and serves as a bifurcation diagram. Each branch is distinguished by its symmetry. The geometry and basic 2D flow have $O(2)$ symmetry in the periodic spanwise direction z , i.e., translations $z \rightarrow z + z_0$ and reflections $z \rightarrow -z$. In the (x, y) plane, they have centrosymmetry $(x, y) \rightarrow (-x, -y)$.

The 2D branch loses stability via a circle pitchfork bifurcation at $Re_{CP} = 228$, breaking the translation symmetry in z . The critical spanwise wavelength is approximately $\lambda = 4.8$ and the critical wavenumber $\beta = 1.3$. The circle pitchfork bifurcation is subcritical, and so the 3D states created branch leftwards and are

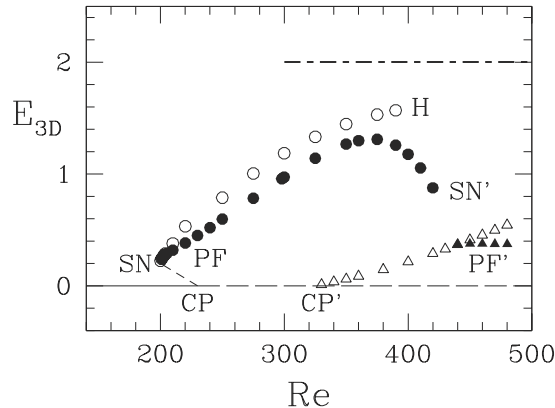


Figure 1. Bifurcation diagram for perturbed plane Couette flow with ribbon height $\rho = 0.086$. Horizontal line: 2D states exist for all Re ; they are stable for $Re < Re_{CP} = 228$. Short-dashed line (schematic): unstable symmetric states with spanwise wavelength λ exist between $Re_{SN} = 197$ and $Re_{CP} = 228$. Hollow circles: symmetric states with λ exist between $Re_{SN} = 197$ and $Re_H = 395$; they are stable between Re_{SN} and $Re_{PF} = 201$. Filled circles: asymmetric states with λ exist between $Re_{PF} = 201$ and $Re_{SN'} = 420$. Hollow triangles: symmetric states with $\lambda/2$ exist for $Re > Re_{CP'} = 330$. Filled triangles: asymmetric states with $\lambda/2$ exist for $Re > Re_{PF'} = 440$. Heavy long-and-short-dashed line (schematic): turbulent states occur for $Re > Re_{CH} = 300$.

unstable; we cannot calculate them with the methods used here. These states have reflection symmetry in z and centrosymmetry in (x, y) ; we call them 3D symmetric states. The centrosymmetry can be visualized as follows: At the ribbon location at $x = 0$, four small vortices are present. The upper two vortices persist for $x > 0$, while the lower two persist for $x < 0$.

The 3D branch changes direction and is stabilized by a saddle-node bifurcation at $Re_{SN} = 197$. Its stability is short-lived, however, lasting only until a pitchfork bifurcation at $Re_{PF} = 201$. The pitchfork bifurcation creates new stable branches with only the pointwise symmetry $(x, y, z) \rightarrow (-x, -y, -z)$; we call these 3D asymmetric states. Figure 2 illustrates this symmetry breaking by showing two different velocity fields at $Re = 240$. The symmetric 3D field on the left has two different reflection symmetries, satisfying both $u(x, y, -z) = u(x, y, z)$ and $u(-x, -y, z) = -u(x, y, z)$. The asymmetric 3D field on the right satisfies only the single reflection symmetry $u(-x, -y, -z) = -u(x, y, z)$. The difference between symmetric and asymmetric 3D fields can also be seen in Figure 6 discussed below. Although the symmetric 3D branch is unstable, we can continue to calculate it by imposing reflection symmetry in z . It is further destabilized, however, by a Hopf bifurcation at $Re_H \approx 395$, beyond which we have not followed it.

The asymmetric 3D branches change direction and are destabilized by a second saddle-node bifurcation at $Re_{SN'} \approx 420$. Surprisingly, time-dependent simulation at $Re = 450$ from an initial asymmetric state at $Re = 400$ leads to a metastable state with half the imposed wavelength of $\lambda = 4.8$, or equivalently, twice the wavenumber of $\beta = 1.3$. The evolution in time of the energies E_1 and E_2 in the β and 2β spanwise Fourier components is shown in Figure 4. The initial field at $Re = 400$ and the metastable state at $Re = 450$ are shown in Figure 3. This transition is *symmetry-restoring* since the field is invariant under translation in z by $\lambda/2$. The metastable state persists during $4300 \lesssim t \lesssim 5800$, when E_1 is near zero.

The metastable state is the $\lambda/2$ branch created from the 2D branch by a circle pitchfork bifurcation at $Re_{CP'} = 330$; see Figure 1. Calculations show that it branches rightwards. Each of the halves of the field is symmetric under reflection in z about its midplane $z = \lambda/4$ or $z = -\lambda/4$. The $\lambda/2$ branch undergoes another pitchfork bifurcation at $Re_{PF'} = 440$, analogous to that undergone at Re_{PF} , creating branches which do not have this reflection symmetry. From Figure 3, it can be seen that the vortices in the $\lambda/2$ field remain somewhat circular; their cross-channel height is reduced along with their spanwise extent. The absence of vortices near the upper and lower walls could indicate that the streamwise velocity profile is more stable in this region than that near the center.

When the $\lambda/2$ branch is created at $Re_{CP'}$, it is necessarily unstable to wavelength doubling in a domain of size λ , because its parent 2D branch is already unstable to λ modes. We are able to calculate the $\lambda/2$ branch from its creation at $Re_{CP'}$ (and, for $Re > Re_{PF'}$, its asymmetric version) by using a domain of size $\lambda/2$. How-

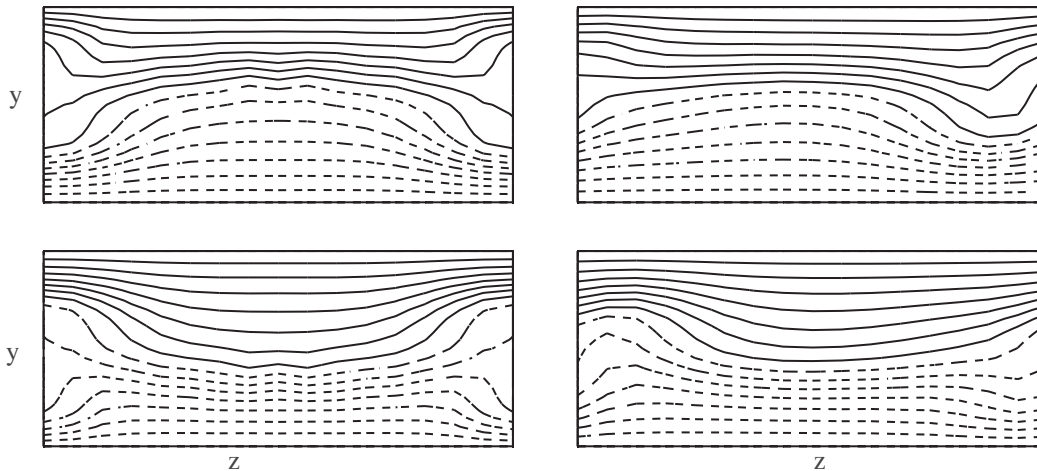


Figure 2. Two velocity fields at $Re = 240$, illustrating breaking of reflection symmetry in z . Contours of streamwise velocity u are shown at $x = 2$ (above) and at $x = -2$ (below). Left: State with reflection symmetry in z and centrosymmetry in (x, y) . For $x = 2$, deformation of u contours shows that w velocity is upwards at mid- z . Thus vortex on left (right) is counterclockwise (clockwise). For $x = -2$, the direction of w and vortex orientation are reversed. Right: State with only the pointwise symmetry $(x, y, z) \rightarrow (-x, -y, -z)$.

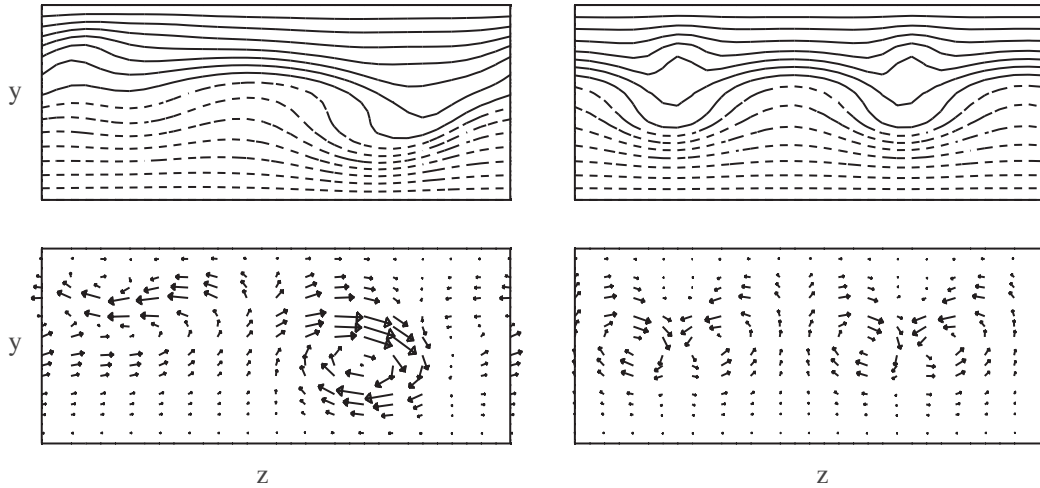


Figure 3. Velocity fields at $Re = 400$ and $Re = 450$ illustrating symmetry-restoring transition. Contours of streamwise velocity u are shown above and (v, w) velocity field vectors are shown below, both at $x = 2$. Left: Asymmetric state with spanwise wavelength $\lambda = 4.8$ at $Re = 400$. The asymmetry in z is very pronounced. Right: Metastable state with spanwise wavelength $\lambda/2 = 2.4$ at $Re = 450$. The vortices occupy only the central portion in y .

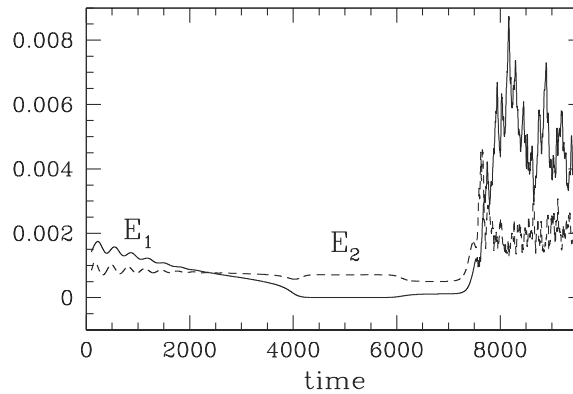


Figure 4. Time evolution of energy in the spanwise Fourier components $\beta(E_1, \text{solid curve})$ and $2\beta(E_2, \text{dashed curve})$ at $Re = 450$. The initial state is the asymmetric β state at $Re = 400$. E_1 decreases to near-zero levels for $4300 \lesssim t \lesssim 5800$; during this interval, the flow is in a metastable state with wavenumber 2β . For $t \gtrsim 7500$, the flow undergoes large-amplitude irregular oscillations, corresponding to turbulence.

ever, we emphasize that during its appearance as a metastable state, it is calculated in the full domain of size λ , i.e., it has been stabilized to wavelength doubling. We propose a possible mechanism for this stabilization: At $Re_{SN'}$, the asymmetric λ branches change direction and stability. If the unstable asymmetric λ branches terminate on the symmetric $\lambda/2$ branch in a subcritical pitchfork bifurcation $Re_{PF''}$, then the symmetric $\lambda/2$ branch will be stabilized to λ perturbations for $Re > Re_{PF''}$, as will the asymmetric $\lambda/2$ branch for $Re > Re_{PF'}$.

However, this bifurcation scenario sheds no light on the subsequent evolution from the metastable $\lambda/2$ state to irregular oscillations, as shown in Figure 4 for $t \gtrsim 7500$. Irregular oscillations persist when the Reynolds number is reduced until $Re < Re_{CH} = 300$, where the flow reverts to the steady asymmetric λ branch. We believe these states correspond essentially to the turbulent flow observed in unperturbed plane Couette flow for $Re \gtrsim 325$ (Lundbladh and Johansson, 1991; Tillmark and Alfredsson, 1992; Daviaud *et al.*, 1992; Hamilton *et al.*, 1995), both because of the closeness of the lower bound in Reynolds number, and because of their appearance and streamwise extent (see Figure 6). Because lack of resolution can produce spurious time dependence, we have verified that these dynamics persist with increased numerical resolution.

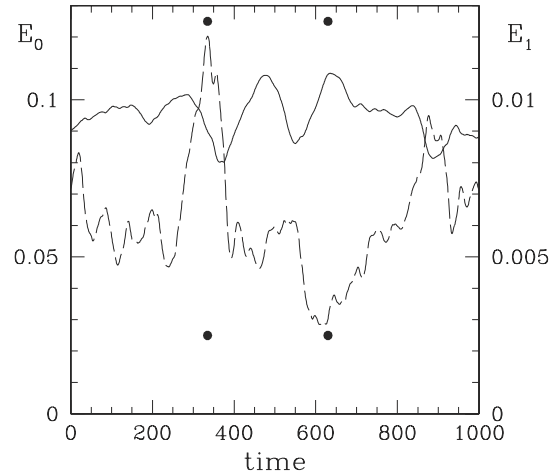


Figure 5. Evolution of energy E_0 (solid curve) and E_1 (dashed curve) in the zero and β spanwise Fourier modes for a turbulent state at $Re = 350$. Dots at $t = 355$ and $t = 630$ show times at which instantaneous streamwise velocity contours are plotted in Figures 6 and 7.

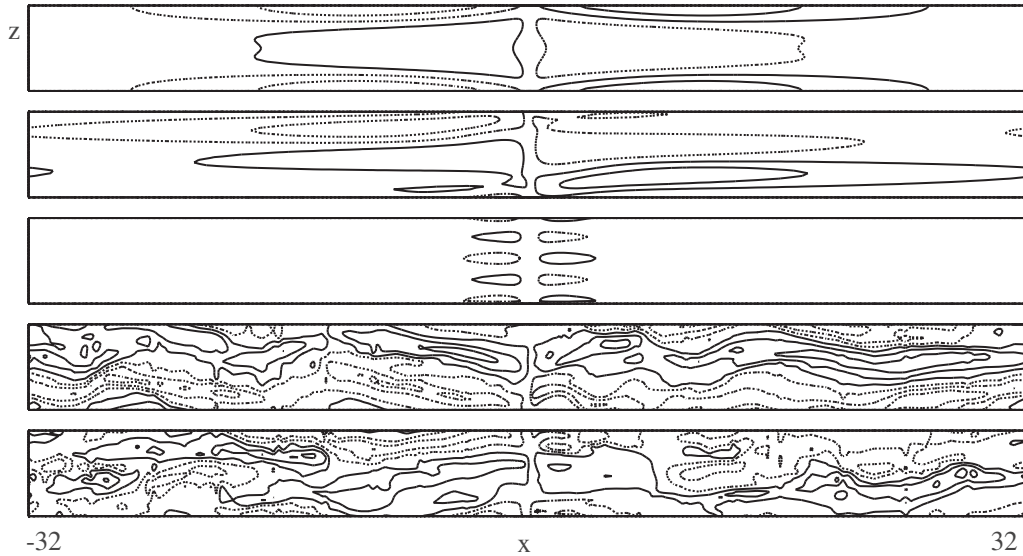


Figure 6. Streamwise velocity contours at $Re = 350$ in the $y = 0$ midplane. Shown from top to bottom are the symmetric, the asymmetric, and the $\lambda/2$ steady states, instantaneous turbulent fields at $t = 355$ and $t = 630$ where E_1 is locally maximal and minimal, respectively.

Figure 5 shows the evolution of the energy E_0 and E_1 in the zero and β spanwise Fourier components at $Re = 350$. Turbulent states at $Re = 350$ are illustrated via streamwise velocity contours in Figures 6 and 7. Figure 6 shows the symmetric, asymmetric, and $\lambda/2$ steady states, in the (x, z) midplane ($y = 0$), as well as two instantaneous snapshots of turbulent states $t = 355$ and $t = 630$, where E_1 is locally maximal and minimal, respectively (see Figure 5). Figure 7 shows the asymmetric steady state and two instantaneous snapshots of turbulent states at $t = 355$, 630 in the (x, y) midplane ($z = 0$). The deviation from plane Couette flow is highly localized around the wire at $x = 0$ for the steady states, but extends over the entire streamwise domain for the turbulent states.

In the experiments (Bottin *et al.*, 1997, 1998), streamwise vortices are observed for $Re > 150$, compared with our threshold of $Re = 200$. Their wavelengths are between 5.2 and 5.7, compared with our critical $\lambda \approx 4.8$. Intermittency is observed experimentally for $Re > 280$ and turbulence for $Re > 325$, in close agreement with our observation of $Re > 300$. Spatial period-halving events are also observed in the experiments

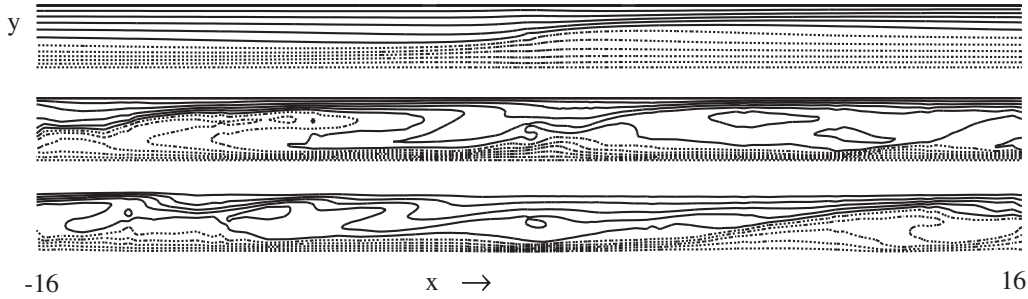


Figure 7. Streamwise velocity contours at $Re = 350$ in the $z = 0$ plane in the central half of the domain. Shown from top to bottom are the asymmetric steady state and instantaneous turbulent fields at $t = 355$ and $t = 630$ where E_1 is maximal and minimal, respectively.

(Dauchot, private communication), as in our transition from the λ to the $\lambda/2$ metastable state. This period-halving transition should be amenable to bifurcation-theoretic analysis.

4. Smaller Ribbons

An important question is the dependence of this scenario on ribbon height ρ . Results from calculations performed for two smaller heights, $\rho = 0.071$ and $\rho = 0.043$, are given in Table 1. For both of these ribbon heights, the 2D flow undergoes a circle pitchfork bifurcation to a 3D eigenmode. Because the critical wavenumber, denoted by β_c , changes very little with ρ , we have given more precise values for $\beta_c(\rho)$ in Table 1 in order to specify the ρ dependence. The fact that β_c is relatively insensitive to ρ provides evidence for the idea that this instability arises from the underlying unperturbed plane Couette flow rather than depending sensitively on the perturbing ribbon. (We have used the same domain with spanwise periodicity $\lambda = 2\pi/(1.30)$ to calculate all secondary bifurcations.) The critical Reynolds number Re_{CP} increases as ρ decreases, as expected from the absence of linear instability at finite Re for plane Couette flow. Both aspects of the ρ -dependence of the transition to three dimensionality are also observed in the experiments.

For $\rho = 0.071$, the bifurcation scenario is similar to that at $\rho = 0.086$. Re_{SN} increases more slowly as ρ decreases than does Re_{CP} , lending support to the hypothesis that branches of steady 3D states might continue to exist as ρ approaches zero, although disconnected from the 2D branch. However, $Re_{SN'}$ decreases, so that the Reynolds number range over which *stable* steady 3D states exist is smaller, as is also observed experimentally. Specifically, the branch of unstable 3D states bifurcating subcritically from the 2D flow occupies the Reynolds number range $Re_{CP} - Re_{SN}$, which increases from 31 for $\rho = 0.086$ to 65 for $\rho = 0.071$, while the branches of stable 3D states occupy the Reynolds number range $Re_{SN'} - Re_{SN}$ which decreases from 223 for $\rho = 0.086$ to 147 for $\rho = 0.071$. We note that Nagata (1990, 1998) and Faisst and Eckhardt (2000) have attempted to compute steady states of plane Couette flow containing streamwise vortices by continuing Taylor vortex flow. In the plane Couette flow limit, they find that the solutions which persist are analogues of wavy Taylor vortex flow, here streamwise traveling waves, and exist for $Re > 125$.

For $\rho = 0.043$, we have been unable to find any stable steady 3D states, despite extensive searching. Thus Table 1 lists only the primary instability Re_{CP} and β_c for $\rho = 0.043$. We observe irregular oscillations for all the initial conditions, Reynolds numbers, and spatial resolutions we have tried. This is in contrast to the experiments (Bottin *et al.* 1997, 1998), in which approximately steady states containing streamwise vortices are

Table 1. Dependence of bifurcations on ribbon height ρ . See Figure 1 and text for a description of the bifurcation sequence. All secondary bifurcations (i.e. all but Re_{CP}) have been calculated in a domain of spanwise periodicity length $2\pi/(1.30)$.

ρ	β_c	Re_{CP}	Re_{SN}	Re_{PF}	$Re_{SN'}$	Re_H
0.086	1.28	228	197	202	420	395
0.071	1.30	283	218	218	365	395
0.043	1.45	538				

observed for ρ even smaller than 0.043. Calculations at intermediate ribbon heights would clarify whether, when, and how the stable steady 3D states disappear as ρ is reduced.

Acknowledgments

We gratefully acknowledge Ron Henderson for the use of `Prism`.

References

- Barkley, D., and Tuckerman, L.S. (1999). Stability analysis of perturbed plane Couette flow. *Phys. Fluids* **11**, 1187–1195.
- Bottin, S., Dauchot, O., and Daviaud, F. (1997). Intermittency in a locally forced plane Couette flow. *Phys. Rev. Lett.*, **79**, 4377–4380.
- Bottin, S., Dauchot, O., Daviaud, F., and Manneville, P. (1998). Experimental evidence of streamwise vortices as finite amplitude solutions in transitional plane Couette flow. *Phys. Fluids*, **10**, 2597–2607.
- O. Dauchot, private communication.
- Daviaud, F., Hegseth, J., and Bergé, P. (1992). Subcritical transition to turbulence in plane Couette flow. *Phys. Rev. Lett.*, **69**, 2511–2514.
- Faisst, H., and Eckhardt, B., (2000). Transition from the Couette–Taylor system to the plane Couette system. *Phys. Rev. E*, **61**, 7227–7230.
- Hamilton, J.M., Kim, J., and Waleffe, F. (1995). Regeneration mechanisms of near-wall turbulence structures. *J. Fluid Mech.*, **287**, 317–348.
- Henderson, R.D., and Karniadakis, G.E. (1995). Unstructured spectral element methods for simulation of turbulent flows. *J. Comput. Phys.*, **122**, 191–217.
- Lundbladh, A., and Johansson, A.V. (1991). Direct simulation of turbulent spots in plane Couette flow. *J. Fluid Mech.*, **229**, 499–516.
- Nagata, M. (1990). Three-dimensional finite-amplitude solutions in plane Couette flow: bifurcation from infinity. *J. Fluid Mech.*, **217**, 519–527.
- Nagata, M. (1998). Tertiary solutions and their stability in rotating plane Couette flow. *J. Fluid Mech.*, **358**, 357–378.
- Tillmark, N., and Alfredsson, P.H. (1992). Experiments on transition in plane Couette flow. *J. Fluid Mech.*, **235**, 89–102.